1 Introduction

Orbital angular momentum (OAM) is a special property of certain beams of light, called optical vortex beams, which appear as ring-shaped intensity distributions around a dark core. The existence of OAM in optical vortices was first predicted by Allen *et al.* in 1992 [1]. The OAM of such beams is quantified as $l\hbar$ per photon, where l is the topological charge of the beam [1]. This property was directly demonstrated by He *et al.* who focused an optical vortex beam onto microscopic particles: absorption of this light transfers OAM and thereby exerts a torque on the particles [2].

This ability to transfer angular momentum from light to a particle has important consequences in optical tweezers, a device that uses a tightly focused beam to trap and manipulate microscopic particles [3]. Optical tweezers have numerous applications, including the capability to probe the viscoelastic properties of DNA, characterize the forces of molecular motors, or transport and modify cells precisely [4]. An optical vortex tweezers adds an additional dimension of rotational control to the regular three dimensional manipulation of a traditional tweezers. The capacity for angular manipulation opens the way for research in many areas such as microfluidic systems, where precisely controlled circulating particles can mix and pump small amounts of liquid, or micromachines, where rotating particles can be used as actuators or generators of kinetic energy [4].

The purpose of the current research was to create an optical vortex beam suitable for use in the inverted optical tweezers which was developed in an earlier stage of our work [5]. While investigating possible methods of making such a beam, we recently discovered a novel and significantly simplified method for creating an optical vortex from a rectangularly symmetric (Hermite-Gaussian) beam. We decided to shift the focus of the overall project to this novel design that may prove helpful to other researchers in the field, and which has considerable mathematical appeal.

The new mode converter requires only one cylinder lens instead of the two carefully spaced ones in the classic design described by Beijersbergen *et al.* in 1993 [6]. Drawbacks of the classic design include the difficulty in matching the input beam to the two astigmatic elements and the need for very careful alignment. Several alternative designs have been proposed to address

these shortcomings, but they introduce additional complexity and as many as six lenses [7, 8]. In the new design described here, the strong astigmatism created by the single cylinder lens is exactly balanced by an astigmatism created by tilting the usual spherical mode-matching lens away from its normal position perpendicular to the beam direction. The discovery of this possibility followed from the chance observation that a dark-core beam could still be produced from the classical mode converter [6] when one of its two cylinder lenses was removed. Upon further investigation by way of spreadsheet models, ABCD matrix analysis and ray traces, the chance observation was explained and the design was modified to accommodate problems like continued astigmatism. The new simplified design offers many advantages: alignment is much quicker and easier as there is only one element that needs to be positioned, sensitivity to deviations is reduced, and power loss and aberrations are minimized by the decrease in optical surfaces.

The device was tested using Hermite-Gaussian (HG) beams produced in two different ways: 1) by inserting a thin wire into the cavity of a low-power open-cavity helium-neon laser, or 2) by introducing a π phase shift into one half of a normal Gaussian beam (HG_{00} mode) from a higher-power He-Ne laser [9]. Successful mode conversions were routinely and easily achieved. The method is so reliable that it can be used as a test for "false" HG beams that were occasionally observed.

Finally, the simplified single-lens mode converter (SLMC) was incorporated into the previously developed inverted optical tweezers setup [5], and the resulting optical vortex tweezers was successfully used to rotate (exert a torque on) 1–2 μm copper oxide particles. The optical vortex character of the converted beam was independently verified by observing the expected characteristic "forked" interference pattern in a Mach-Zehnder interferometer.

2 Background

2.1 Transverse Laser Modes

Laser beams are defined by the paraxial approximation of the electromagnetic wave equation:

$$\nabla^2 U - \frac{1}{c^2}\frac{\partial^2 U}{\partial t^2} = 0 \tag{1}$$

where ∇ is the del operator, U is a scalar field, and c is the speed of light. A transverse laser mode is simply a specific solution to this equation based on the boundary conditions imposed by the laser cavity. There are two major classes of transverse laser modes: the Hermite-Gaussian (HG) modes and the Laguerre-Gaussian (LG) modes.

2.1.1 Hermite-Gaussian Modes

HG modes are rectangularly symmetric solutions to the paraxial wave equation and can be expressed as:

$$U_{m,n}^{HG}(x,y,z) = C_{m,n}^{HG}\frac{1}{w}\exp\left[-\frac{ik(x^2+y^2)}{2R} - \frac{x^2+y^2}{w^2} - i\psi(z)\right] \times H_m\left(\frac{x\sqrt{2}}{w}\right)H_n\left(\frac{y\sqrt{2}}{w}\right) \quad (2)$$

where H_m is a Hermite polynomial, z is the distance from the beam waist, $R(z) = z\sqrt{1+(z/z_0)^2}$ is the wavefront radius of curvature, $w(z) = w_0\sqrt{1+(z/z_0)^2}$ is the size of the beam waist, and the Rayleigh range of the beam, or the area around the beam waist where the light rays are relatively parallel, is defined as $z_r = \frac{\pi w_0^2}{\lambda}$ [10]. z_r is important in relation to $\psi(z)$, the term for the Gouy phase shift, which will be described in detail later. HG modes are described by two indices m and n which describe the number of nulls along the horizontal and vertical axis of the beam's cross-section, respectively. An HG_{00} mode, or normal Gaussian mode, is simply a single circular spot, shown as $\exp[\frac{-x^2-y^2}{w^2}]$, the most familiar output from a well-behaved laser.

The simplest way to create true HG modes is through an open-cavity gas laser. Inserting a thin wire inside the laser cavity changes the original boundary conditions and favors the formation of higher-order modes. (We actually used a a thin hair measured to be 50 μm from its diffraction pattern.) Careful manipulation of the mirrors will change the angle of the beam, and various higher order HG modes can be created in this manner.

However, there are other methods of approximating an HG mode. For example, an HG_{10} mode is a beam with its two halves mutually π out of phase and destructively interfering in the center. This can be simulated by introducing a phase element to dissect the beam into two halves [9]. The phase element is adjusted, using an interferometer, to create an exact π phase shift, as shown in Figure 1. Yet, this synthetic HG mode is merely an approximation of a true HG mode. Due to effects like edge diffraction from the phase element, the resulting mode is actually a superposition of several higher-order HG modes [9].

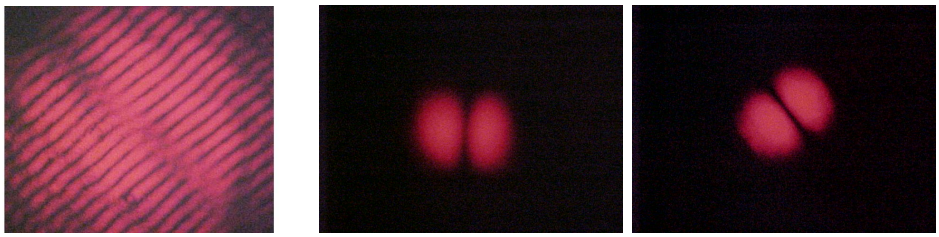

Figure 1: One half of a synthetic HG_{10} mode is π radians out of phase as shown by the displacement of fringes in the pattern from a Mach-Zehnder interferometer (left). A synthetic HG_{10} mode (center) and a true HG_{10} mode (right) appear similar in the far-field.

2.1.2 Laguerre-Gaussian Modes

LG modes are circularly symmetric solutions to the paraxial wave equation which can be expressed as:

$$U_{l,p}^{LG}(r,\phi,z) = C_{l,p}^{LG}\frac{1}{w}\exp\left[-\frac{ikr^2}{2R} - \frac{r^2}{w^2} - il\phi - i\psi(z)\right] \times \left(\frac{r\sqrt{2}}{w}\right)^l L_p^l\left(\frac{2r^2}{w^2}\right) \tag{3}$$

where L_p^l is a Laguerre polynomial. LG modes are generally described by two indices p and l, where $p+1$ is the number of nulls encountered radially and l is the topological charge of the beam, or the number of 2π cycles the beam's phase undergoes around its cross-section [10]. In other words, as described by the $\exp(il\phi)$ term, the phase of an LG mode varies along with its azimuthal angle ϕ (for $l \neq 0$). Optical vortices are basically $l \neq 0$ LG modes that are enclosed within a beam.

As the beam's phase varies, the magnitude of its electric and magnetic fields vary too, causing the Poynting vector $\vec{S}(\vec{r})$, which is $\frac{1}{\mu_0}\vec{E}(\vec{r}) \times \vec{B}(\vec{r})$, to vary too. When all points of equal phase are connected in an optical vortex mode, a helix is formed (see Figure 2). As a result, the Poynting vector spirals along this helix. In the process, it gains a component tilted with respect to the direction of the beam's propagation. The time average of the component of the Poynting vector in the xy-plane, in general, is zero. However, this new azimuthal component remains and in turn creates a net angular momentum $\vec{J}$ in the beam, proportional to $\vec{S} \times \vec{r}$ [11]. The azimuthal component is termed orbital angular momentum (OAM) and it is an intrinsic property of optical vortex modes. It is this property that is exploited in optical tweezers to rotate particles.

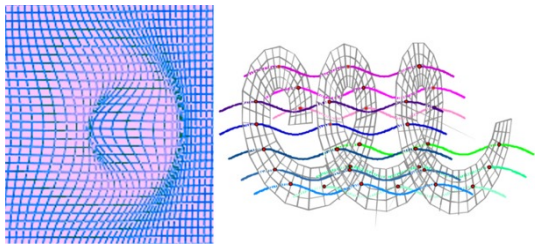

Figure 2: When the points of equal phase in an LG mode are connected, a helical wavefront is formed [12]. Consequently, the Poynting vector acquires an azimuthal component, resulting in OAM.

2.2 Matrix Optics

Matrix optics is an important analytical tool used to trace the path of a beam by generalizing the beam into a few key rays. This sort of ray optics model works well except in the vicinity of a focus, where the size of the beam is determined by its wave nature, through diffraction.

The initial ray is described by its height and angle relative to the z-axis as a two-component vector, $\begin{bmatrix} y_1 \\ \theta_1 \end{bmatrix}$. The resultant vector, $\begin{bmatrix} y_2 \\ \theta_2 \end{bmatrix}$, is then determined by multiplying 2×2 ray optic matrices with the initial vector. As a ray travels through a system of optical elements, a composite matrix for the entire system can be obtained by multiplying the individual matrices for each element, $\mathrm{M}_{\mathrm{composite}} = \mathrm{M}_x\mathrm{M}_{x-1}...\mathrm{M}_2\mathrm{M}_1$. In this work, matrices are used to model beam propagation through free space, $\begin{bmatrix} 1 & d \\ 0 & 1 \end{bmatrix}$, and through thin lenses of focal length f, $\begin{bmatrix} 1 & 0 \\ -\frac{1}{f} & 1 \end{bmatrix}$ [13].

2.3 Gaussian Optics

The Gaussian or wave-optic model considered in this section correctly treats the diffraction effects near a focus. The same 2×2 ray matrices described in the earlier section are used. The initial beam, however, is described by a complex q-parameter instead of a two-component vector. It is given by $q = z + iz_r$, where z is the distance along the z-axis from the focus of the beam and z_r is the Rayleigh range of the beam. When a beam passes through some optical element, its ray matrix elements are used to calculate a new q-parameter: $q_2 = \frac{Aq_1+B}{Cq_1+d}$ where A, B, C, and D are matrix elements a_{11}, a_{12}, a_{21}, and a_{22} respectively. Moreover, knowing the q-parameter of the beam, it is possible to calculate the radius of curvature and beam width by $\frac{1}{q_1} = \frac{1}{R(z)} - \frac{2i}{kw(z)^2}$ [13].

Each optical element in the system has to be calculated individually and the matrices cannot be multiplied to produce one system matrix, as in the ray optic model. To facilitate calculations, a Microsoft Excel spreadsheet model was created. Starting with an input q-parameter, it iteratively calculates the new beam parameters, including z, z_r, $R(z)$, and $w(z)$, through a series of ABCD matrices. This model has many advantages, including the capability of easily inserting specific optical elements at any point to see how each beam parameter changes, and the ability to plot the beam width at every point through a system (see Figures 7 and 12).

2.4 Gouy Phase Shift

The ψ term in the HG and LG equations refers to the Gouy phase shift. Basically, when a beam goes through a focus, it undergoes a phase shift as the beam is retarded by the change in radius of curvature. The phase shift is described by $\psi = \arctan \frac{z}{z_r}$. The theoretical limit to the Gouy shift, as the beam approaches and exits a focus from/to infinity, is $\arctan \frac{\infty}{z_r} - \arctan \frac{-\infty}{z_r} = \pi$.

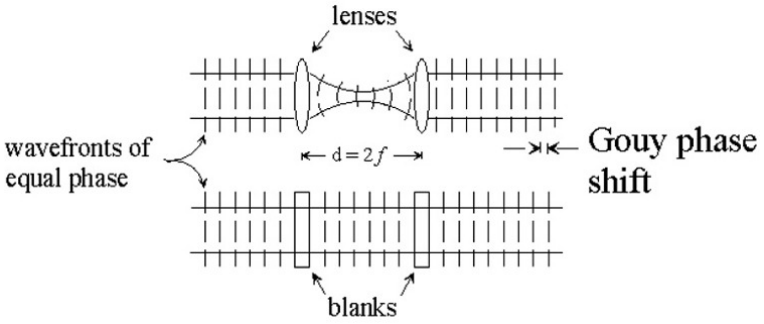

Figure 3: As the beam focuses, its phase is retarded by the change in wavefront curvature [12].

2.5 Experimental Techniques

Many experimental techniques were employed in the course of this project, the most significant ones being the measurement of the Rayleigh range of lasers, the construction of interferometers, and alignment of optical elements. To determine the Rayleigh range, the beam's radius $w(z)$ was measured at five or six distances from the laser using the pinhole method. A 100 μm diameter pinhole was translated across the width of the beam, 10 μm at a time, while a photodetector recorded the intensity at each point. The Rayleigh range of the beam is then calculated by finding the hyperbolic beam profile that best matched the data points. This technique was used on both the open-cavity laser (z_r = 300 mm) and the large 33 mW laser used for the

vortex tweezers ($z_r = 1100$ mm). Mach-Zehnder interferometers were constructed to verify the vortex nature of the beam created by the mode converter [11]. The reference beam was either a plane wave or a mirror image of the vortex created by placing a dove prism in one arm of the interferometer. Alignment techniques for the setups were described in our previous paper [5].

3 Laser Mode Converters

The HG and LG families of modes, in linear algebraic terms, are two independent complete basis sets of solutions to the paraxial wave equation. Therefore, transformations exist between the two basis sets, as noted by Tamm and Weiss [14]. This is the key concept of mode converters.

3.1 Transformation between HG and LG modes

If Equation (3) for an LG_{lp} mode is rewritten as an LG_{mn} mode with its topological charge $l = |m-n|$ and radial index $p = \min(m, n)$, a mathematical relationship can be established between these LG $_{mn}$ modes and HG_{mn} modes, described by Equation (2). This relationship can be described most elegantly by splitting the HG_{mn} mode into its components in a coordinate system that is rotated $\frac{\pi}{4}$ radians from the original. For example, $\mathrm{HG}_{10}(x, y, z) = \mathrm{HG}_{10}(\frac{x\sqrt{2}}{2}, \frac{y\sqrt{2}}{2}, z) + \mathrm{HG}_{01}(\frac{x\sqrt{2}}{2}, \frac{y\sqrt{2}}{2}, z)$. Moreover, mode $\mathrm{LG}_{10} = \mathrm{HG}_{10}(\frac{x\sqrt{2}}{2}, \frac{y\sqrt{2}}{2}, z) + i\mathrm{HG}_{01}(\frac{x\sqrt{2}}{2}, \frac{y\sqrt{2}}{2}, z)$. In other words, an LG_{10} mode consists of the same components as an HG_{10} mode, except that the two components are relatively out of phase by $\frac{\pi}{2}$ radians. Thus, for all the beams considered here, an HG_{mn} mode can be transformed into an LG_{mn} mode by relatively phase shifting its vertical and horizontal components by $\frac{\pi}{2}$ radians, in a coordinate plane rotated by $\frac{\pi}{4}$ radians [6].

3.2 Traditional Mode Converter

The basic setup of a mode converter, as described by Beijersbergen *et al.* [6], uses an input HG_{mn} mode which is a superposition of component modes rotated $\frac{\pi}{4}$ radians, and exploits the Gouy phase shift to create a relative $\frac{\pi}{2}$ phase shift between these components to produce an LG_{mn} mode. As previously mentioned, the Gouy phase shift of a beam is proportional to $\arctan\frac{z}{z_r}$. By changing the Rayleigh range, z_r, of one axis of the beam, it is possible to create a phase shift between the two axes. This is accomplished in a system of three lenses. Two cylinder lenses are used in one axis, one to create the astigmatism that causes the phase shift, and one to make the beam isotropic (circular or non-astigmatic) again. An additional mode-

matching lens adjusts the Rayleigh range of the input beam to ensure the correct net difference in phase shift between the two axes [6]. In order to achieve the correct phase shift and have an

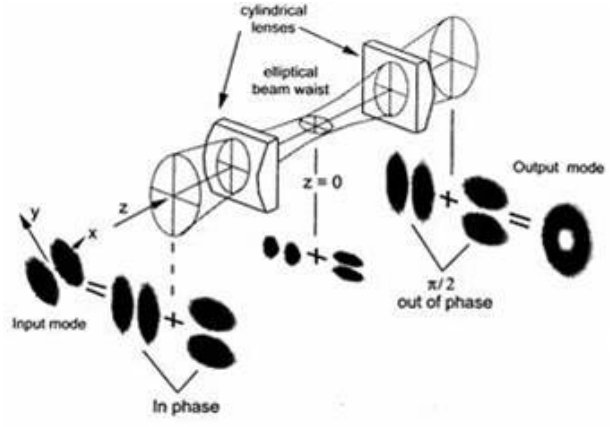

Figure 4: Traditional mode converter setup, as described by Padgett *et al.* [15]. The input beam is adjusted by a mode-matching lens that is not depicted above.

isotropic output beam, several conditions need to be met. For a converter using cylinder lenses of focal length f and separation d:

1. The radii of the input and output beams should be equal: $\frac{{z_{rx}}^2+d^2}{z_{rx}} = \frac{{z_{ry}}^2+d^2}{z_{ry}}$.
2. The beam should be mode-matched for f: $\frac{1}{f} = \frac{1}{R_x} - \frac{1}{R_y} = \frac{d}{{z_{rx}}^2+d^2} - \frac{d}{{z_{ry}}^2+d^2}$.
3. The net Gouy phase shift must be $\Delta\psi = \frac{\pi}{2}$.

When these conditions are met, the separation between the two cylinder lenses of focal length f is calculated to be $f\sqrt{2}$ and a mode-matching lens is selected such that its Rayleigh range is $f(1+\frac{1}{\sqrt{2}})$. Such a mode converter was created using two plano-convex cylinder lenses of $f = 20$ mm, $d = 2.8$ mm, and a mode-matching lens of $f = 100$ mm at the output of an open-cavity laser. Several different orders of HG modes were successfully converted (see Figure 5).

3.3 The New Single-Lens Mode Converter (SLMC)

Much difficulty is often encountered in determining an appropriate mode-matching lens and properly spacing and aligning the optical elements in the traditional mode converter [15]. While experimenting with these parameters, the creation of a dark-core beam without the use of a second cylinder lens was noted. A Mach-Zehnder interferometer was constructed to observe the interference pattern of this beam with a reference plane wave, and the same was done for the

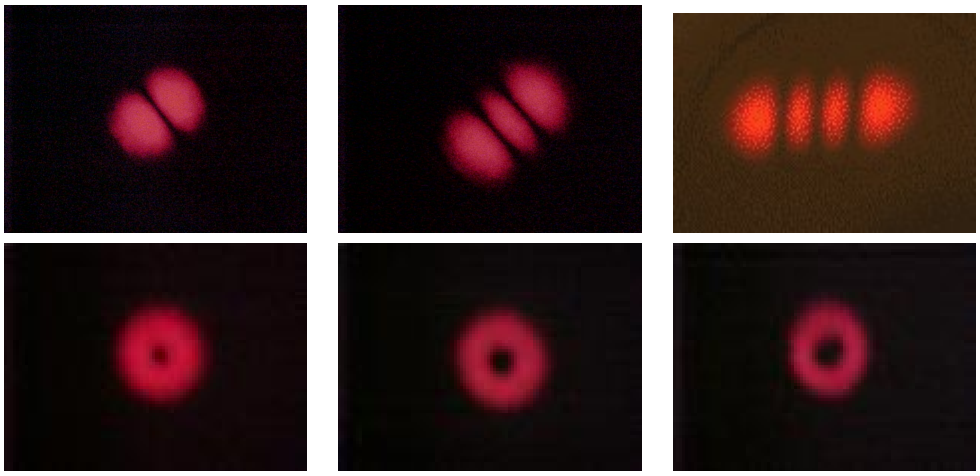

$HG_{10} \Rightarrow LG_{10}$ $HG_{20} \Rightarrow LG_{20}$ $HG_{30} \Rightarrow LG_{30}$

Figure 5: Mode Conversions achieved with a traditional mode converter

known vortex from the traditional converter. Both interferograms showed a clear fork with 2 prongs, proving both beams to be $l = 1$ vortices (see Figure 6). This ability to perform a mode

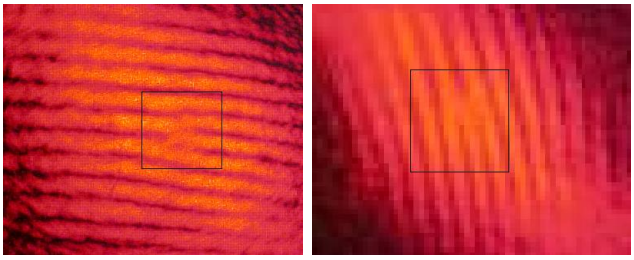

Figure 6: Interference patterns of beams showing forks with 2 prongs, proving that the beams are both $l = 1$ vortices. Traditional mode converter (left); SLMC (right).

conversion with one cylinder lens can be explained by noting that this lens is placed a short distance after the focus of the input beam. Consequently, one axis goes through a second focus and another Gouy phase shift. When the lens is placed at the proper distance, the net shift equals $\frac{\pi}{2}$ and an optical vortex is created. However, the lack of a second cylinder lens causes the beam to remain astigmatic. Consequently, as the beam propagates, the two axes diverge at different rates and the beam becomes elliptical. For example, the appropriate phase shift is achieved when the mode-matching lens and the cylinder lens are placed 108 mm and 308.5 mm from the laser, respectively. The beam's propagation through such a system is graphed in Figure 7 using the spreadsheet model described earlier. To solve this problem, additional

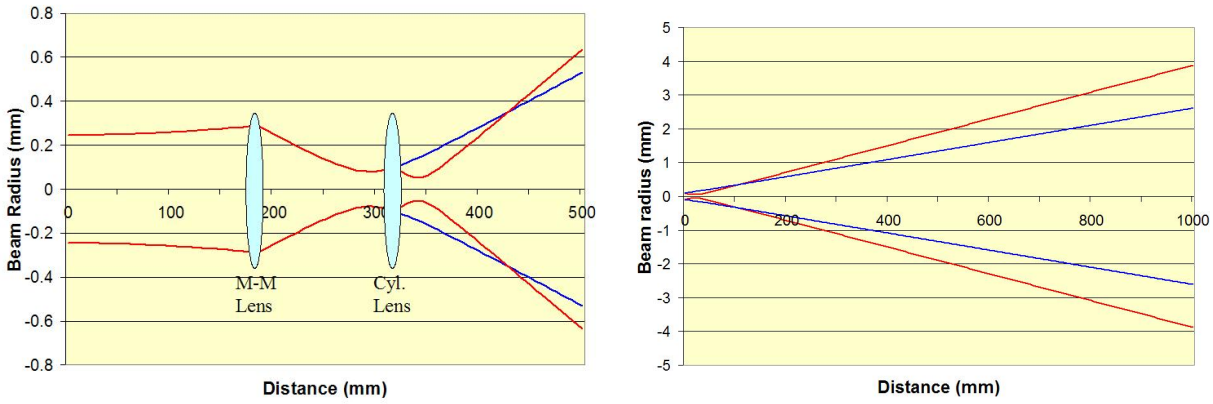

Figure 7: The radii of the x-axis (blue) and the y-axis (red) are graphed as the beam propagates through the mode converter (left), and directly after exiting the mode converter (right). The beam remains astigmatic and very elliptical as it propagates.

astigmatism has to be induced in the x-axis to balance that produced in the y-axis. This can be achieved by tilting the existing spherical mode-matching lens, or rotating it around its vertical axis. The tilt causes the beam's horizontal axis to cross more glass than its vertical axis and the focal length of the x-axis is thereby reduced (see Figure 8). Using this property of tilted lenses,

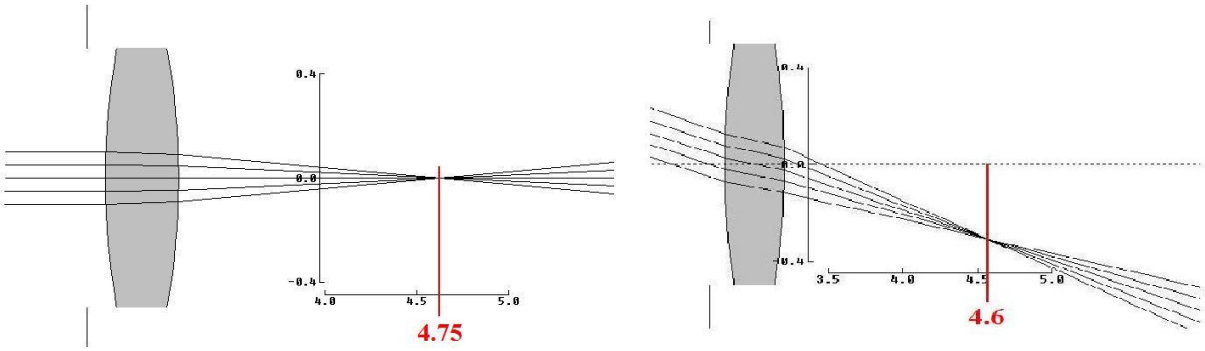

Figure 8: The BEAM2 ray trace program from Stellar Software can be used to model the astigmatism created in a tilted lens. The y-axis remains unaffected (left) while the x-axis focal length is reduced (right) from 4.75 to 4.6 units. In reality, the tilt angle is much larger.

an SLMC with an isotropic output beam was constructed by following the iterative procedure outlined below:

1. The mode-matching lens was initially set perpendicular to the beam's propagation.
2. An input HG beam at a $\frac{\pi}{4}$ angle to the normal coordinate plane was created and the cylinder lens was moved until a proper phase shift of $\frac{\pi}{2}$ was achieved and a vortex created.

3. The laser was then adjusted to produce a normal Gaussian mode and the mode-matching lens was tilted until the output beam appeared circular in the far-field (see Figure 9).

4. Steps 2 and 3 were repeated until a circular optical vortex was created from the SLMC.

Successful mode conversions were achieved in this manner (see Figure 10).

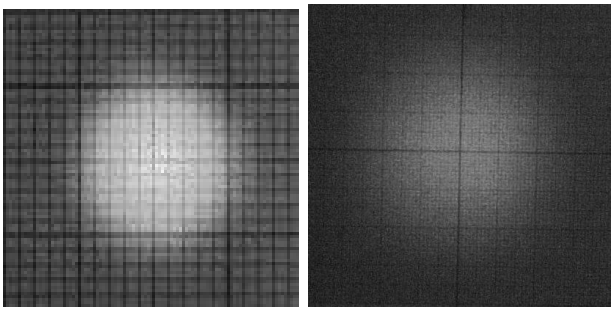

Figure 9: The output of an SLMC with an input Gaussian beam is shown at a distance of 1650 mm and at a distance of 8000 mm. Note that the beam retains a circular appearance as it propagates.

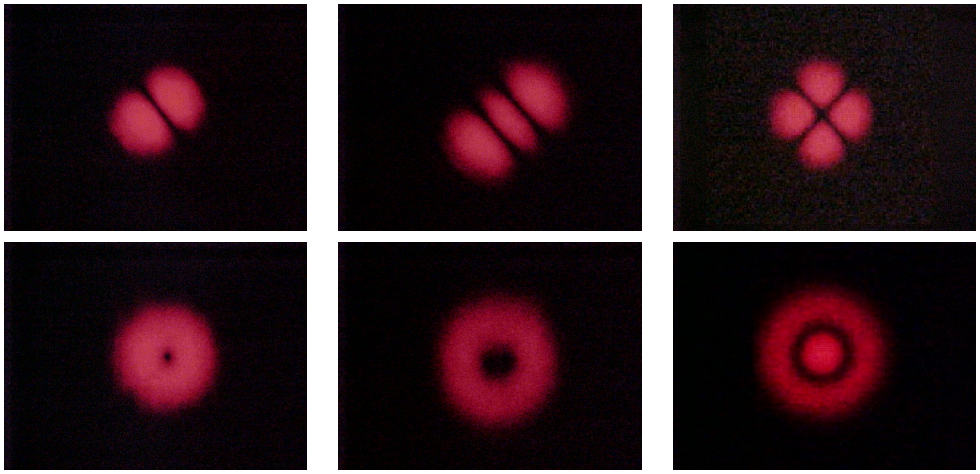

$HG_{10} \Rightarrow LG_{10}$ $HG_{20} \Rightarrow LG_{20}$ $HG_{11} \Rightarrow LG_{11}$

Figure 10: Mode Conversions achieved with the new Single-Lens Mode Converter (SLMC).

3.4 A Mathematical Model of the SLMC

The two conditions that need to be met to achieve a successful mode conversion and an isotropic output beam can be modeled using mathematics from Sections 2.2 - 2.4. Consider an SLMC consisting of a mode-matching lens with an effective focal length f_2 for the tilted axis and a

regular focal length f_1, a cylinder lens with focal length f_3, a lens separation of distance d, and an input beam of q-parameter q_0. As illustrated in Figure 11, the following must hold true:

1. Any beam obtains a new Rayleigh range or divergence after passing through a lens. The final Rayleigh range of the x- and y-axes need to be equal so that the beam diverges at the same rate along either axis. Thus, the $\mathrm{Im}(q_1)$ or z_{r1} obtained after the beam q_0 travels through the matrix for lens f_1 in the x-axis, should equal the $\mathrm{Im}(q_3)$ or z_{r3} after the beam travels through the matrices for lens f_2, distance d, and lens f_3.

2. The net difference in Gouy phase shift between the two axes must be $\frac{\pi}{2}$. The net phase shift of the x-axis is $\psi_1 + \psi_2$. The net phase shift of the y-axis is $\psi_3 + \psi_4 + \psi_5 + \psi_6$. Since ψ_2 and ψ_6 are equivalent to $\arctan(\frac{s}{z_r})$ where s is the propagation of the beam beyond the mode converter and $s >> z_r$, both these values are approximately equal to $\frac{\pi}{2}$ and do not affect the net difference in phase shift between the two axes. Thus, the condition can be written as $-\arctan\frac{-f_1}{z_{r1}} + \frac{\pi}{2} = -\arctan\frac{-f_2}{z_{r2}} + \arctan\frac{d-f_1}{z_{r2}} - \arctan\frac{-f_3}{z_{r3}}$.

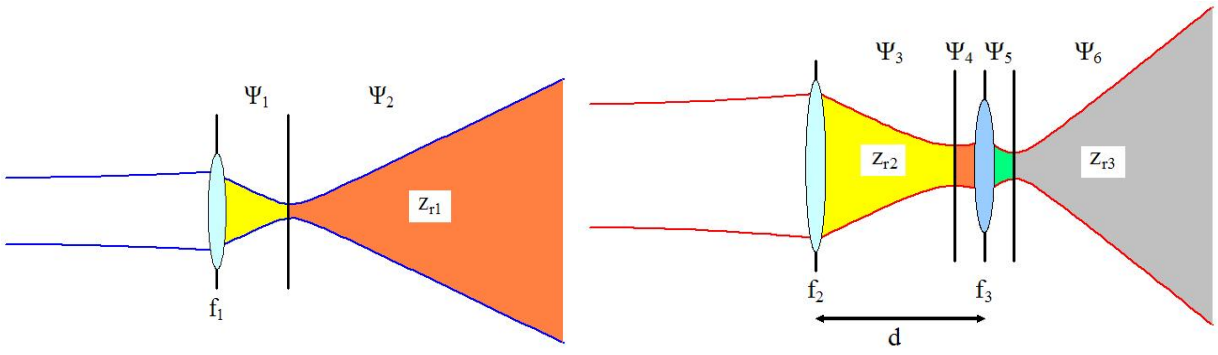

Figure 11: The x-axis of the beam (left) travels through a tilted lens of effective focal length f_1. Its phase shift is $-\psi_1 + \psi_2$ and its final Rayleigh range is z_{r1}. The y-axis of the beam (right) travels through a lens of focal length f_2, a distance of d, and a second lens of focal length f_3. Its phase shift is $-\psi_3 + \psi_4 - \psi_5 + \psi_6$ and its final Rayleigh range is z_{r3}.

For example, these parameters are satisfied by the SLMC, used to achieve the mode conversions in Figure 10, where the $f = 100$ mm mode-matching lens is placed 180 mm away from the laser and the $f = 20$ mm cylinder lens is placed a further 130 mm away. The input beam has initial q-parameter $q_0 = 180 + 300i$. In the y-axis, it is sent through the following matrices: $\begin{bmatrix} 1 & 0 \\ -\frac{1}{100} & 1 \end{bmatrix}$, $\begin{bmatrix} 1 & 130 \\ 0 & 1 \end{bmatrix}$, and $\begin{bmatrix} 1 & 0 \\ -\frac{1}{20} & 1 \end{bmatrix}$. The output beam's q-parameter is then calculated to be $q_3 = -20.7 + 12.8i$ in the vertical axis. Thus, the beam's x-axis Rayleigh range must also equal 12.8 mm. Since the x-axis of the beam is not affected by the cylinder lens, the

mode-matching lens can be rotated around a vertical axis in the simulation to find the point at which a Gaussian input beam appears circular in the far-field. The horizontal-axis focal length where this condition was achieved was 66 mm, about $\frac{2}{3}$ of the original 100 mm focal length. The x-axis of the beam, described by the same input q-parameter q_0, thus travels through the matrix $\begin{bmatrix} 1 & 0 \\ -\frac{1}{66} & 1 \end{bmatrix}$. Finally, both axes of the output beam travel through free space for a distance s as described by the matrix $\begin{bmatrix} 1 & s \\ 0 & 1 \end{bmatrix}$. The x- and y-beam radii as the beam propagates are graphed in Figure 12 using the spreadsheet model. Though the beam is initially elliptical, as the y-axis goes through a second focus, this feature becomes increasingly insignificant as the beam propagates through a significant distance with both axes maintaining the same divergence or Rayleigh range (see Figure 12). The net difference in phase shift between the two axes can be calculated by $[-\psi_3 + \psi_4 - \psi_5] - [-\psi_1] = [-\arctan\frac{-108.3}{31.1} + \arctan\frac{23.2}{31.1} - \arctan\frac{-21.3}{12.7}] - [-\arctan\frac{-70.8}{12.7}] = 1.57 \approx \frac{\pi}{2}$. Thus, the appropriate phase shift is achieved and a mode conversion with a non-astigmatic output is produced.

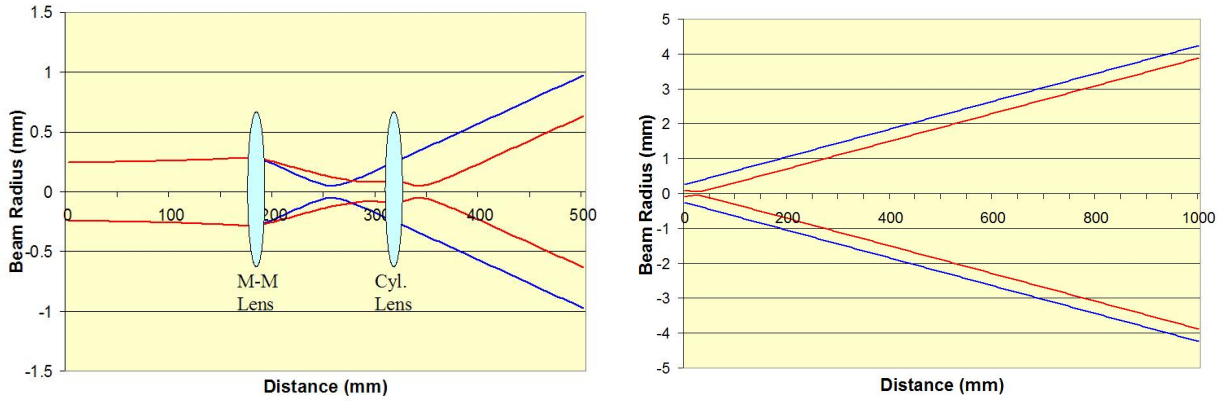

Figure 12: The beam radii $w(z)$ along the x-axis (blue) and the y-axis (red) are graphed as the beam propagates through the mode converter (left), and directly after it exits the mode converter (right). The difference between the two beam radii becomes increasingly insignificant as the beam propagates, resulting in an almost perfectly circular beam.

A key advantage of the SLMC is its ease of alignment, due to the reduction of optical elements, and its decreased sensitivity to deviations. In the aforementioned example, a net relative phase shift of $\frac{\pi}{2}$ is achieved when the cylinder lens is placed 180.5 mm away from the laser. However, an acceptable phase shift is achieved even when the lens is displaced by a few millimeters. The phase shift achieved as the beam is displaced from its ideal position at 180.5

mm is graphed below in Figure 13; the relationship is quite linear within the given region. This relative insensitivity to position allows great flexibility in alignment and placement.

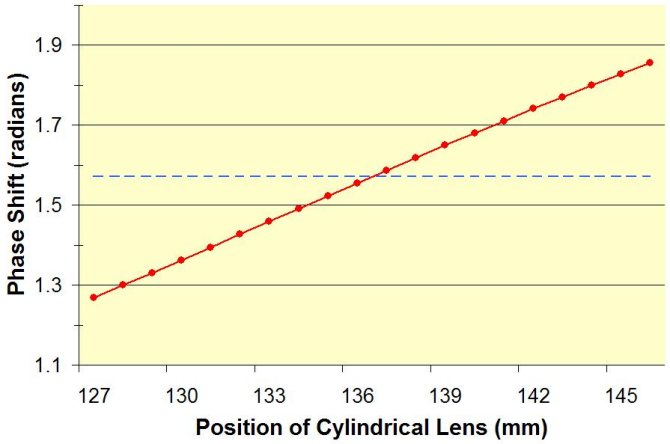

Figure 13: The net relative phase shift between the x- and y-axes as a function of the cylinder lens' position. The blue dotted line shows the desired phase shift of $\frac{\pi}{2}$.

4 Application to Optical Tweezers

Since a high-power open-cavity laser was not available to create an HG mode for use in our optical tweezers, a synthetic mode was created from a high-power closed-cavity laser instead (see Section 2.1.1). The mode created in this manner is not ideal but this is not related in any way to the use of the SLMC (see Figure 14). A streak is observed in the vortex created due to the edge diffraction from the phase element. The beam also appears rather elliptical because of "invisible vortices" that appear on the sides; this is due to the fact that the HG approximation is actually an overlap of several different orders of HG modes [9]. However, as shown in the interference pattern in Figure 6, the resulting beam is indeed a true l=1 optical vortex. Having

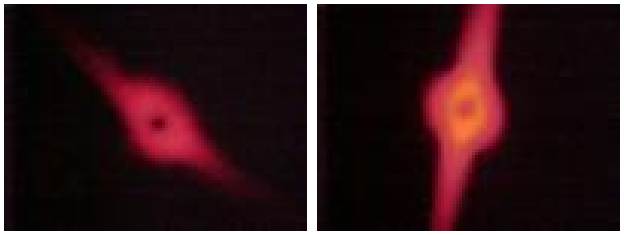

Figure 14: A l=1 vortex converted from a synthetic HG mode by a traditional mode converter and an SLMC respectively.

successfully achieved an optical vortex beam of suitably high-power, the previously developed inverted optical tweezers [5] was re-assembled to demonstrate the angular momentum of the vortex by rotational control of microscopic particles.

4.1 Summary of Optical Tweezers Theory

Electromagnetic radiation carries energy and momentum. An interaction between this radiation and matter can result in the transfer of linear momentum to the particle [3]. This principle is the underlying basis of laser-activated traps (optical tweezers) that use a single laser beam to transfer momentum and manipulate micron-sized particles in a fluid medium.

When a light ray passes through a particle, it refracts and the photons' velocity and momentum decrease. The change in momentum exerts a series of forces on the particle that are governed by the direction in which the light refracts - forces act in opposite reactionary pairs so when the particle causes the light to refract down, the light exerts an upward force on the particle. The key forces acting on the particle can be classified as the gradient force, the scattering force, and the force of gravity. The gradient force acts towards the region of highest intensity (the beam's focus) and is responsible for trapping the particle. In an inverted optical tweezers, the other two forces, the scattering force and the force of gravity, oppose each other to minimize their net effect [5] as shown in Figure 15. It is vital that the power of the beam at the plane of

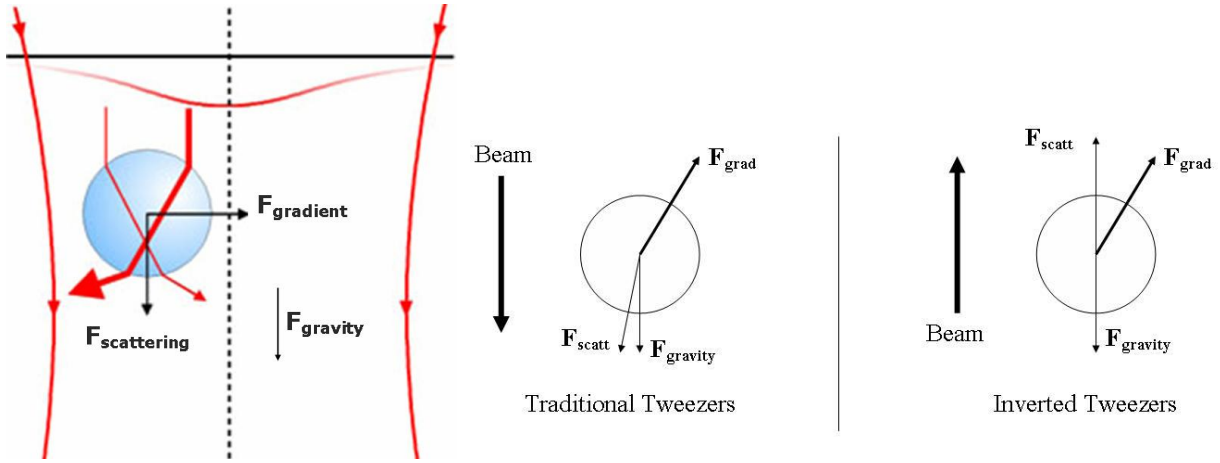

Figure 15: The gradient and scattering forces and the force of gravity are depicted above for a traditional tweezers [16]; the scattering force and gravity act against the gradient force in a traditional tweezers; the scattering force and gravity act against each other in an inverted tweezers.

the focus is high because it is directly proportional to the magnitude of the gradient or trapping force exerted on the particle by the beam. The intensity of the focus can be maximized through careful alignment procedures that ensure that the highest beam intensity enters the aperture of the objective that is used to focus the beam onto a particle. The net force then acting on a particle can be gauged by measuring the maximum velocity at which a particle can be dragged by the tweezers in the fluid medium, commonly known as drag velocity. Drag velocity can be used to calculate the drag force exerted, using Stokes' equation.

4.2 Setup

The setup is depicted in Figure 16. The laser used was a Spectra Physics Model 127 633 nm He-Ne laser with a measured output power and Rayleigh range of 33 mW and 1100 mm respectively. The phase element used to form the synthetic HG mode was a 100 μm thick microscope cover slip at a 45° angle, placed on a rotational and translational stage in order to facilitate achieving the correct position and effective thickness. The SLMC consisted of a $f = 200$ mm mode-matching lens and a $f = 20$ mm cylinder lens. The diverging optical vortex beam was collimated by a 750 mm plano-convex lens at an appropriate diameter ($2w = 5$ mm) to slightly underfill the 6 mm aperture of the objective. A final $f = 170$ mm lens brought the beam to a focus 160 mm away from the objective. The beam is reflected off of a dichroic mirror and sent upwards into the 100x Melles Griot objective to be focused onto the sample chamber on the microscope stage. Meanwhile, the white illumination light from above is transmitted through the dichroic and reflected into a CCD camera for imaging. This is the same arrangement as was previously used to trap and manipulate yeast cells three-dimensionally using a 19.5 mW laser [5].

Small copper (II) oxide from Fisher Scientific were used as the sample particles [2]. Black in color, they absorb the optical vortex beam and its intrinsic orbital angular momentum, making them ideal for demonstrating rotational control.

4.3 Results and Observations

Rotation of $\sim$1 μm diameter copper (II) oxide particles was successfully achieved in the optical vortex tweezers, as shown in Figure 17. The scattering force of the beam pushed the particles against gravity to the top of the sample chamber where their rotational speeds were measured

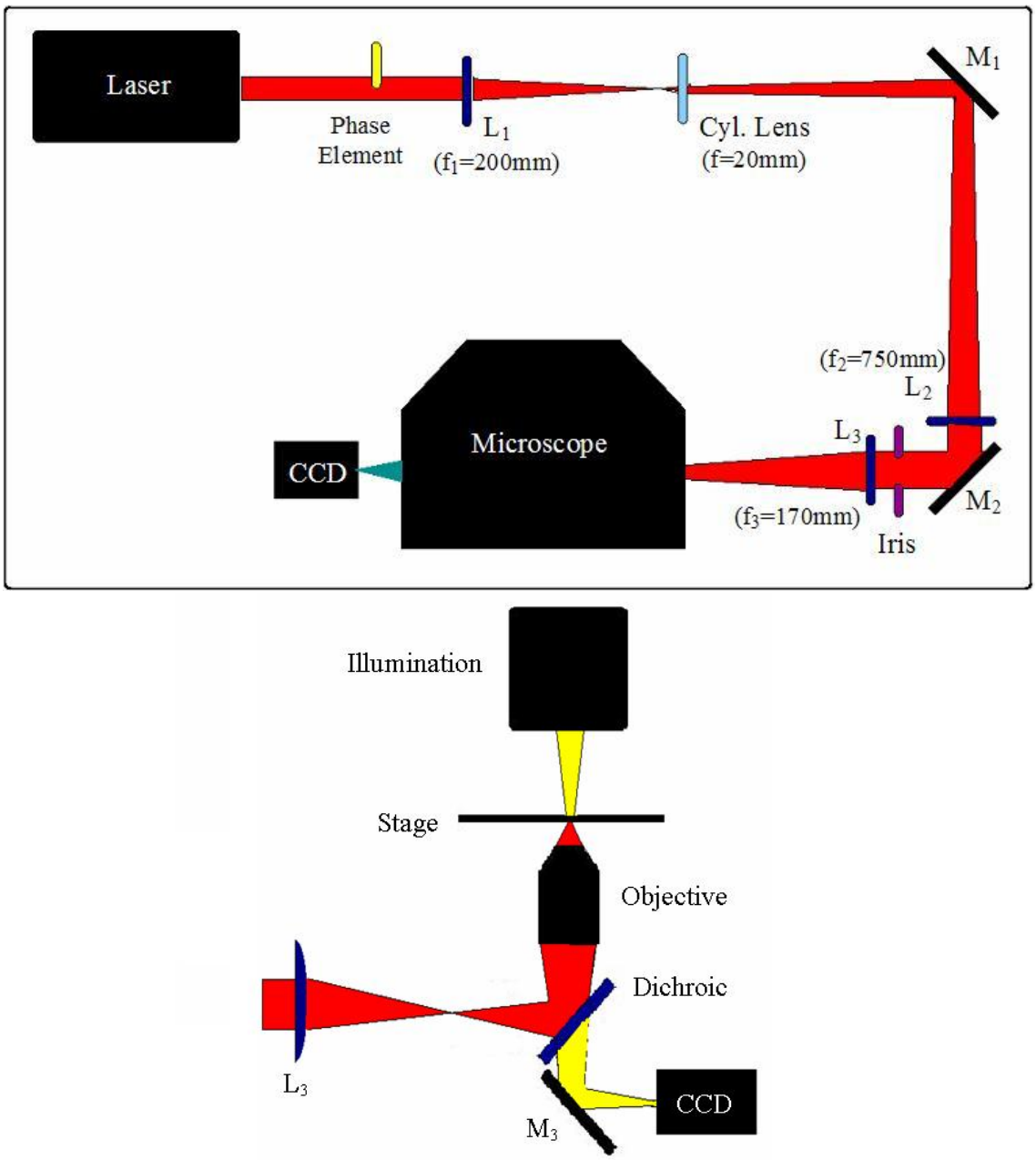

Figure 16: The top and side views of the vortex tweezers setup are shown above. All elements are to scale except the length of the laser (42") and the width of the laser beam.

to be $\frac{\pi}{3}$ radians per second clockwise on average. The net torque exerted on a particle can be calculated to be $\tau = -8\pi\eta r^3\omega$ where η is the viscosity of water ($10^{-3}\frac{\text{kgm}}{\text{s}}$), r is the radius of the particle (10^{-6} m), and ω is the maximum angular velocity ($-\frac{1}{6}$ Hz). Thus, the particle absorbs approximately 4.2×10^{-21} Nm of torque on average. One difficulty encountered was in stably trapping the CuO particles. Unlike yeast cells, these particles are absorptive and are repelled

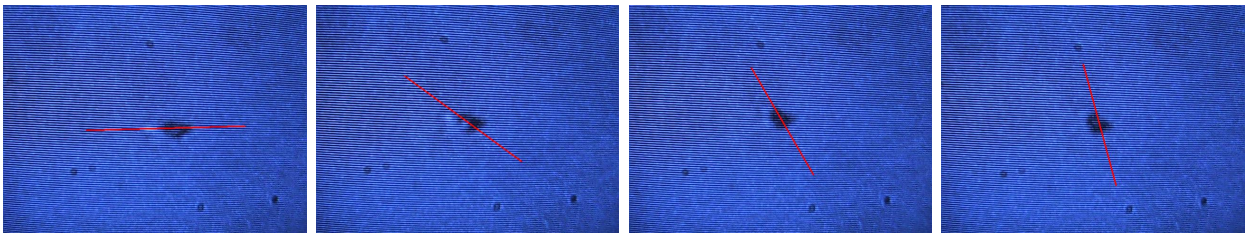

Figure 17: An asymmetric CuO particle is shown rotating $\frac{\pi}{2}$ radians over an interval of 1.5 seconds.

from the high-intensity ring of the beam; they need to be trapped in the dark core of the vortex. This task was made difficult by the fact that the vortex was produced from a synthetic HG mode rather than a true one. Consequently, the beam's focus sometimes appeared as two bright spots (similar in appearance to an HG_{10} mode) instead of a ring, allowing a trapped particle to escape relatively easily. Modifying the laser by inserting a cross-cavity wire to create a true HG_{10} mode might be a future way to overcome this difficulty.

5 Conclusions and Continuing Work

A novel simplified single-lens mode converter (SLMC) has been created for the conversion of Hermite-Gaussian (HG) to Laguerre-Gaussian (LG) modes. The SLMC has been analyzed mathematically and an iterative procedure has been created to assemble one experimentally. Successful mode conversions have been achieved from both true and synthetic HG modes, as confirmed by observing the vortex character of the output modes with an interferometer. Finally, an optical vortex tweezers was constructed, incorporating a synthetic HG mode and the new SLMC. The orbital angular momentum of the vortex was demonstrated by successfully rotating microscopic copper (II) oxide particles.

The workings of the SLMC are still being investigated in an ongoing study of the exact effects of the tilt of the mode-matching lens on the focal lengths along either axis. If this relationship can be quantified, the correct tilt angle for the mode-matching lens can be calculated instead of determined by the current trial and error method. Another area of future investigation is the study of relative trapping efficiency of a vortex beam compared to an HG_{00} mode. Since the vortex beam is annular, the undesirable scattering force is strongly reduced and more intensity is concentrated on the steep rays, which in turn maximizes the gradient or trapping force.

References

[1] L. Allen *et al.*, "Orbital angular momentum and the transformation of Laguerre-Gaussian laser modes," *Phys. Rev. A* **45**, 8185 (1992).

[2] H. He *et al.*, "Direct observation of transfer of angular momentum to absorptive particles from a laser beam with a phase singularity," *Phys. Rev. Lett.* **75**, 826 (1995).

[3] A. Ashkin *et al.*, "Observation of a single beam gradient force optical tap for dielectric particles," *Opt. Lett.* **11**, 288 (1986).

[4] D. Grier, "A revolution in optical manipulation." *Nature* **424**, 810 (2003).

[5] H. Sridhar, "Development of an inverted optical tweezers with full motional control," Submission to Intel International Science and Engineering Fair, May 2007. http://laser.physics.sunysb.edu/∼hamsa/papers/

[6] MW Beijersbergen *et al.*, "Astigmatic laser mode converters and transfer of orbital angular momentum," *Opt. Comm.* **96**, 123 (1993).

[7] AN. Alekseev *et al.*, "Conversion of Hermite-Gaussian and Laguerre-Gaussian beams in an astigmatic optical system. 1. Experiment," *Technical Physics Letters* **24**, 68 (1998).

[8] AA. Malyutin, "Tunable astigmatic $\pi/2$ mode converter," *Quantum Electronics* **34**, 172 (2004).

[9] Y. Yoshikawa and H. Sasada, "Versatile generation of optical vortices based on paraxial mode expansion," *J. Opt. Soc. Am. A* **19**, 2127 (2002).

[10] E. J. Galvez, "Gaussian beams in the optics course." *Am. J. Phys.* **74**, 355 (2006).

[11] E.J. Galvez and Nikolay Zhelev, "Orbital angular momentum of light in optics instruction," Proceedings of the 2007 Education and Training in Optics and Photonics (ETOP) Conference. http://spie.org/etop/2007/etop07fundamentalsIII.pdf

[12] E.J. Galvez, "Light Beams in High-Order Modes," November 2007. http://departments.colgate.edu/physics/research/optics/oamgp/gp.htm

[13] Daniel A. Steck, "Classical and Modern Optics," Optics Course Notes for U. of Oregon (unpublished), November 2007.
http://atomoptics.uoregon.edu/∼dsteck/teaching/optics/optics-notes.pdf

[14] C. Tamm and C. O. Weiss, "Bistability and optical switching of spatial patterns in a laser," *J. Opt. Soc. Am. B* **7**, 1034 (1990).

[15] M. Padgett, J. Arlt, and N. Simpson, "An experiment to observe the intensity and phase structure of Laguerre-Gaussian laser modes," *Am. J. Phys.* **64**, 77 (1996).

[16] S. Block, "Optical Tweezers: An Introduction," November 2007.
http://www.stanford.edu/group/blocklab/Optical%20Tweezers%20Introduction.htm